Physics Letters B 816 (2021) 136256

Contents lists available at ScienceDirect

Physics Letters B

www.elsevier.com/locate/physletb

Direct fusion measurement of the ^{8}B proton-halo nucleus at near-barrier energies

J.C. Zamora [a,*], V. Guimaraes [a], G.V. Rogachev [b,c], S. Ahn [b], J. Lubian [d], E.N. Cardozo [d], E. Aboud [b,c], M. Assuncao [e], M. Barbui [b], J. Bishop [b,c], A. Bosh [b,c], J. Hooker [b,c], C. Hunt [b,c], H. Jayatissa [b,c], E. Koshchiy [b], S. Lukyanov [f], R. O'Dwyer [b,c], Y. Penionzhkevich [f], B.T. Roeder [b], A. Saastamoinen [b], S. Upadhyayula [b,c]

[a] *Instituto de Fisica, Universidade de Sao Paulo, SP 05508-090, Brazil*
[b] *Cyclotron Institute, Texas A&M University, College Station, TX 77843, USA*
[c] *Department of Physics and Astronomy, Texas A&M University, College Station, TX 77843, USA*
[d] *Instituto de Fisica, Universidade Federal Fluminense, Niteroi, RJ 24210-340, Brazil*
[e] *Departamento de Fisica, Universidade Federal de Sao Paulo, Diadema, SP 09913-030, Brazil*
[f] *Joint Institute for Nuclear Research, RU-141980 Dubna, Russian Federation*

ARTICLE INFO

Article history:
Received 25 October 2020
Received in revised form 22 March 2021
Accepted 25 March 2021
Available online 29 March 2021
Editor: B. Blank

ABSTRACT

Direct measurements of the total fusion cross section for $^{8}B + ^{40}Ar$ were achieved with the active target technique. The fusion excitation function was extracted at energies near the Coulomb barrier. The cross section is well described by a coupled reaction channels calculation. The data were compared with previous ^{8}B fusion experiments on ^{28}Si and ^{58}Ni targets. No evidence of striking enhancement of the total fusion cross section at near the Coulomb barrier, that was previously reported for the $^{8}B + ^{58}Ni$ system, was observed in these direct measurements. The present data are systematically consistent with the results for $^{8}B + ^{28}Si$ at higher energies and with other weakly-bound systems at near-barrier energies.

Fusion reactions are the primary energy source of stars and play a fundamental role for the nucleosynthesis in the stellar media [1,2]. Fusion of charged particles ranging from hydrogen, carbon and oxygen contributes to change the chemical composition of the core and they have direct implications in the thermophysical properties of the star [3,4]. The accurate and detailed description of the fusion reaction mechanism is key to understanding the stellar evolution and the abundance of the elements in the universe.

At energies below the Coulomb barrier, the fusion mechanism is based on the fundamental quantum-mechanical tunneling process where particles penetrate through a potential barrier. Besides the importance for astrophysics, this phenomenon plays an essential role in some other subjects such as quantum computing, radioactivity, scanning tunneling microscope and tunnel diode. In nuclear physics, the fusion process occurs when the projectile particle penetrates through the barrier generated by the repulsive Coulomb and attractive nuclear potentials [5]. However, the barriers for heavy-mass systems are complex and depend on the angular momentum and internal degrees of freedom of nuclei. At near-barrier energies, the fusion cross section is strongly influenced by static and dynamic effects, as well as the nuclear structure of the two fusing partners [5–7]. Thus, a proper description of a fusion process requires the use of the coupled-channel (CC) formalism including all the most relevant reaction channels. This makes the situation for weakly-bound nuclei more complex, because of the significant influence of the breakup-reaction channel and strong coupling to the continuum.

As the production of radioactive ion beams became accessible at new accelerator facilities, investigation of fusion reactions involving weakly-bound nuclei has been a subject of great interest in the last years. Extensive experimental and theoretical efforts have been devoted to understand direct reactions involving weakly-bound nuclei as inclusive transfer or breakup at near Coulomb-barrier energies, as well as their influence on the fusion process [8–17]. The low binding energy and strong cluster configuration in halo nuclei produce a decoupling between the valence particle and the core nucleus, which gives rise to an increase of the breakup and/or transfer probability in the total reaction cross section. It has been observed that the coupling of these direct processes affects the total fusion (TF) cross section showing a suppression at energies above the Coulomb barrier and enhancement at sub-barrier

* Corresponding author.
E-mail address: cardona@if.usp.br (J.C. Zamora).

https://doi.org/10.1016/j.physletb.2021.136256

energies when compared with no-coupling one-dimensional barrier penetration [8–12,18,19].

Fusion cross section induced by neutron-halo radioactive beams has been measured for different systems [20–24]. A suppression of the fusion due to breakup effects at energies above the Coulomb barrier and an enhancement at sub-barrier energies have been observed in most of the cases. For proton-halo nuclei, the enhancement of the fusion cross section at energies below the barrier is predicted to be larger than in the neutron case [16]. Coulomb-nuclear interference at very large distances plays an important role in the reaction mechanism because of the extended size of the valence-proton wave function [25,26]. However, fusion data of proton-halo systems are still scarce. For instance, fusion cross section of ^{8}B (proton-halo nucleus) were measured with targets of ^{28}Si [27] and ^{58}Ni [28]. Different results are obtained when data from these experiments are compared with the one-dimensional barrier penetration model. A small suppression above the barrier was observed for the $^{8}B + ^{28}Si$ system (similar to neutron-halo data), while the $^{8}B + ^{58}Ni$ system presents a very large enhancement below and above the barrier with respect to systematics for tightly-bound nuclei. However, the interpretation of these results is not simple, since both experiments rely on particle-evaporation yields and their analysis are highly-model dependent.

In this Letter, we present an innovative experimental approach to investigate fusion for the $^{8}B + ^{40}Ar$ system with direct measurements using the active target technique. The fusion excitation function is unambiguously extracted at near-barrier energies. The evaluation of these model-independent data is fundamental to understand the fusion mechanism involving proton-halo nuclei.

A secondary ^{8}B beam was produced in-flight using the ^{6}Li(^{3}He, n)^{8}B reaction and the Momentum Achromat Recoil Spectrometer (MARS) at the Cyclotron Institute at Texas A&M University [29]. The primary ^{6}Li beam was accelerated via the K150 Cyclotron to an energy of 9.9 MeV/u and transported to the cryogenic gas target located at the entrance of MARS. The gas-cell target was filled with ^{3}He at a pressure of 800 Torr and temperature of 77 K. A 97%-pure 5.1 MeV/u ^{8}B beam of 10^{3} pps was produced with an energy spread of 1.2 MeV. The main contaminants were ^{6}Li and ^{4}He with intensities of 2% and 1%, respectively.

The beam was transported to the TexAT (Texas Active Target) [30] scattering chamber installed downstream at the end of the MARS line. A vacuum-tight 4-μm thick Havar window was placed at the entrance of the scattering chamber to separate the TexAT gas volume from the beam line. The TexAT detector setup consists of a gas-filled Time Projection Chamber (TPC) with a MICROMEGAS (Micro-MEsh GAseous Structures) detector [31] using 1024 read-out channels on an active area of 224×240 mm^2. A windowless ionization chamber (IC) was mounted near the scattering chamber entrance window for particle identification on an event-by-event basis and overall normalization. In addition, a 5×5 cm^2 silicon detector (1 mm thick) was installed at zero degrees at the end of the scattering chamber to monitor the unreacted beam particles.

The TexAT scattering chamber was filled with a gas mixture of ^{40}Ar (95%) + CH_4 (5%) [P5] at 150 Torr that was adjusted to almost stop the unreacted ^{8}B particles in the gas and enable about 1 MeV signal in the silicon detector. An uniform electric field of 29 V/cm was produced by a negative potential of -800 V applied to the cathode plate on top of the field cage of TexAT. The electron drift velocity in the gas was calculated to be 38 mm/μs using MAGBOLTZ [32]. To reduce the read-out rate of the TPC and avoid a considerable dead time for the data acquisition, an external trigger was generated from the IC and micromesh signals with a veto composed by the silicon detector and the last eight MICROMEGAS channel layers (in the central region). This configuration allowed to record only reaction events which were completely detected inside the TPC and remove all the unreacted beam particles and scattering below 16 degrees (relative to the beam direction). The absolute normalization was obtained by integrating the accepted ^{8}B beam rate and the respective target thickness derived from the online gas-pressure monitor. An integrated luminosity of 2×10^{27} cm^{-2} was achieved over 80 hours of beam-on-target. Reactions on ^{12}C were subtracted from the data with measurements using a pure CH_4 (methane) gas target at 180 Torr.

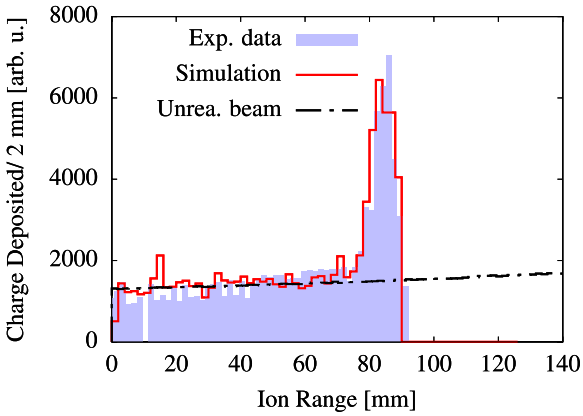

Fig. 1. Ionization beam profile for a typical fusion event. A fusion event deposits a large amount of charge in a short range. The experimental data is compared with a realistic simulation of a fusion event with a sequential α-particle evaporation.

Reaction events were reconstructed from the 3-dimensional hit information of the TPC. The x-y coordinates are determined from the projection on the MICROMEGAS pad plane, while the z coordinate is obtained from the electron drift time [30]. Hit pattern of individual events were analyzed with the RANSAC (RANdom SAmple Consensus) [33] algorithm to classify the particle tracks (inliers) and reject uncorrelated points (outliers) [34]. The algorithm has a wide range of applications in computer vision, and also it has been successfully employed in the analysis of other TPC experiments as AT-TPC [35] and ACTAR [36]. This procedure allowed to identify and fit the 3D linear tracks for the beam and the reaction products. The ionization beam profile (Bragg curve) was extracted for each event using energy deposition along tracks in the TPC. A large and strongly localized charge deposition is produced by a fusion event due to creation of heavy and high Z recoil, up to Vanadium, that looses all its energy over the range of few cm in the gas. That is, the fused particle induces a large-charge signal in a few pixels, which generates a significant increase in the Bragg-peak amplitude. A typical fusion event is shown in Fig. 1.

The maximum amplitude of these distributions exceeds about 4 times the charge deposited by the unreacted beam, as it is predicted from realistic simulations using the TexATSim package [37]. A simulation of a fusion reaction (red curve) with a sequential α-particle evaporation is presented in Fig. 1. The width and total amplitude of the Bragg peak depends mainly on the fusion residue and to the respective momentum kick of the particle. Thus, fusion reactions were isolated from contamination of scattering events by analyzing the shape (amplitude, width and derivative) of the peaks. Evaporated particles were also observed in the experiment, similar as reported in Refs. [38,39]. Charged-particle evaporation (e.g. α) from the fused system was identified in some events with tracks emerging from the region of the Bragg peak. The gas gain of the MICROMEGAS detector was set low to keep the large signals produced by fusion events within the dynamic range of GET electronics [40] that was used for the readout. As a result, the low ionization produced by proton tracks in the gas was not sufficient to get the signal above the threshold. Therefore, proton evaporation that followed fusion events were indistinguishable from neutron evaporation in this experiment.

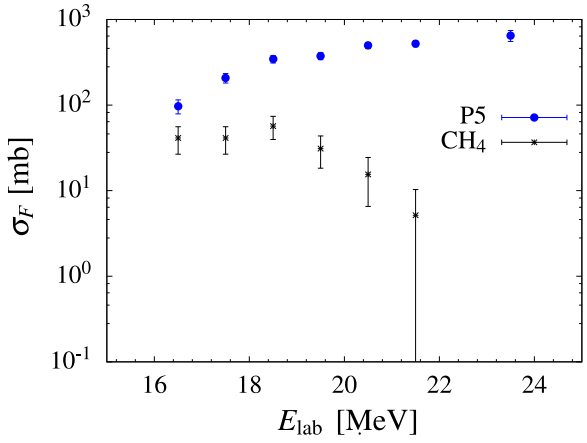

Fig. 2. Fusion excitation function for measurements with P5 and CH_4 gas targets. The CH_4 measurements are employed to subtract a small component of fusion on ^{12}C from P5 data.

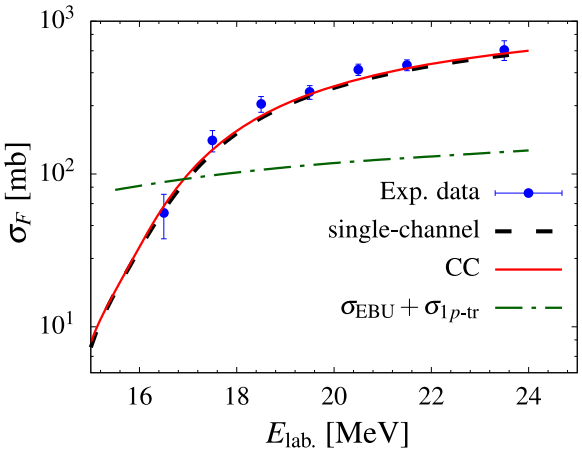

Fig. 3. Total fusion excitation function for ^{8}B + ^{40}Ar. The experimental data is compared with the theoretical fusion cross sections obtained from single channel and coupled channel calculations. Theoretical cross section for the sum of elastic breakup and one-proton transfer channels is shown with a dash-dotted green curve. (see the text for details).

The fusion excitation function was extracted from the ^{8}B range that was integrated in intervals of 1 cm width. The ion range was converted to energy by using stopping power tables calculated with the code SRIM [41]. The target thickness was calculated with the gas-pressure readout and realistic gas density obtained from a thermophysical properties database [42]. The energy losses in the entrance window and dead volume in the scattering chamber allowed for an incident beam energy of 25.8 MeV in the active region. The absolute normalization of the cross section was extracted from the accepted trigger rate and the gas-pressure monitor. The systematic error associated with the normalization was dominated by the integrated beam rate and it was calculated to be ∼12%. Fig. 2 shows the total fusion excitation function for P5 (^{40}Ar [95%] + CH_4 [5%]) and methane (CH_4) gas targets.

Fusion in the ^{8}B + ^{40}Ar system is the dominant contribution in the cross section, however a small component of fusion with ^{12}C is expected to be present in the data (due to the 5% of methane) [39]. Thus, additional runs with a pure-methane gas target were measured to subtract the contribution of ^{12}C. The gas pressure and electric field were adjusted accordingly in order to keep similar conditions as with the P5 target. Very few ^{8}B + ^{12}C fusion events that could contaminate the excitation function were observed and they primarily concentrate below 19 MeV (laboratory frame). Different than expected, the yield at higher energies is quite low, but with a statistical uncertainty in the order of 30%. A limitation in the detection efficiency in the respective active region could be a possible reason for the small values of the cross section at these energies. Nevertheless, fusion on ^{40}Ar is more than an order of magnitude higher for $E_{\rm lab.} \geq 19$ MeV. After subtraction with the proper statistical weights that reflect the composition of the gas target, the fusion excitation function for the ^{8}B + ^{40}Ar system is extracted. Fig. 3 shows the respective total fusion cross section at near-barrier energies compared with theoretical calculations.

Theoretical calculations were performed with the coupled reaction channels (CRC) code FRESCO [43]. As a first approximation, a single-channel (potential scattering) calculation that includes only projectile and target ground states was performed. The optical potential (OP) assumed for this calculation is composed by a real part using the parameter-free Sao Paulo potential (SPP) [44] and a short-range Woods-Saxon potential with parameters $W = 50$ MeV (depth), $r_I = 1.06$ fm (reduced radius) and $a_I = 0.2$ fm (diffuseness) for the imaginary part. The latter parameters were chosen to only account for absorption due to fusion. As explained in Ref. [45], a small variation the in Woods-Saxon parameters of the imaginary potential do not significantly impact the fusion cross section. For the ^{8}B + ^{40}Ar system, a 20% change in any of the three parameters produces a difference in the fusion cross section of less than 2%. This confirms that the absorption is kept in the inner region of the Coulomb barrier.

By comparing this calculation with the experimental data, one can put in evidence the entangling effect of all the direct reactions channels, including the breakup. A coupled-channel calculation was performed using the same OP and assuming a collective excitation of ^{40}Ar within the vibrational model with the one and two-phonon quadrupole excited states. The deformation parameter was taken from systematics [46]. The effect of including these collective excitations is rather soft. This is expected since the single-channel calculation already exhausts the TF cross section. Other relevant channels such as elastic breakup (EBU) and transfer were not included in the coupled scheme. In order to evaluate the importance of these reaction channels, continuum-discretized coupled channel (CDCC) and one-proton transfer calculations were performed. The same procedure from Refs. [47–49] was adopted for the present CDCC calculations. One-proton transfer [^{40}Ar(^{8}B, ^{7}Be)^{41}K] cross sections were calculated within the CRC formalism. The same OP used for the single-channel calculation was employed for the entrance partition. In the exit partition, the interaction was obtained from the SPP assuming scaling factors of 1 and 0.78 for the real and imaginary parts, respectively. This is guided by the fact that no couplings were considered in the exit partition. The spectroscopic amplitudes for the target and projectile overlaps were derived from shell-model calculations using the code NUSHELLX [50]. About 20 excited states in ^{41}K up to 3.05 MeV, including the g.s. and first excited state in ^{7}Be, were taken into account for the calculation. The resulting one-proton transfer cross section was almost negligible and accounts only 4% of the EBU yield. For a better comparison with the TF cross section, both components were summed up. The relative small yield of the EBU and one-proton transfer channels might be an indication that dynamic effects are not contributing on the reaction mechanism for the total fusion in the ^{8}B + ^{40}Ar system. However, it should be clarified that there is no direct connection between the probability of exciting a specific channel and its effect on the transmitted flux. An example is the enhancement of the fusion cross section by coupling to kinematically closed channels (see for instance Refs. [51–54]). Another example is the multi-nucleon transfer reaction. The cross section for these channels might be high depending on the Q-value and the spectroscopy of the initial and final states. The main condition to enhance the fusion cross section is that the residual nuclei are more deformed that the initial ones [55–58], which is

Table 1
Barrier parameters employed for the reduction of the TF cross section. These values were extracted from the bare SPP using a numerical interpolation.

Target	R_B [MeV]	V_B [MeV]	$\hbar\omega$ [MeV]	Ref.
^{28}Si	8.15	11.28	3.59	[27]
^{40}Ar	8.57	13.87	3.76	This work
^{58}Ni	8.90	20.83	4.14	[60]

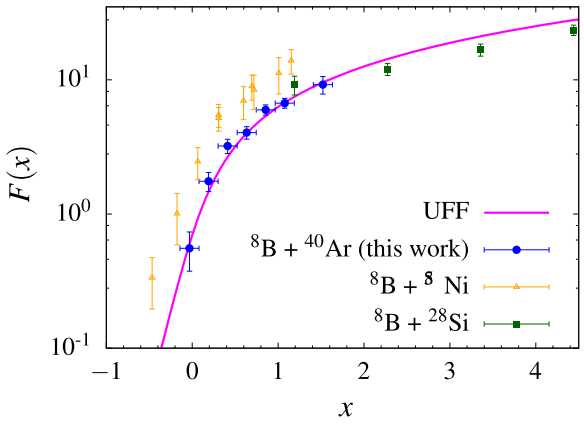

Fig. 4. Reduced total fusion cross section using the Universal Fusion Function (UFF) parameterization. Our data is compared with the experimental results using ^{28}Si [27] and ^{58}Ni [28] targets, and their posterior reanalysis in Ref. [60]. The line (UFF) corresponds to the prediction from the one-dimensional barrier penetration model.

not related to the magnitude of the transfer cross section. At this energy regime, the EBU and the one-proton transfer occur outside the barrier while fusion will only happen if the barrier is tunneled.

A popular method to compare the TF cross section for several systems is from a reduction based on the Universal Fusion Function (UFF) [18,19]. In this method, the energy and cross section are transformed with the parameters $x = (E_{\text{c.m.}} - V_B)/\hbar\omega$ and $F(x) = 2E_{\text{c.m.}}\sigma_F/(\hbar\omega R_B^2)$, where R_B and $\hbar\omega$ are the radius and curvature of the barrier, respectively. An advantage of this transformation is that the TF cross section is directly compared with the reduced Wong's function [59] (UFF), which is the prediction of the one-dimensional barrier penetration model. The barrier parameters employed for the reduction of the TF cross sections were extracted from the bare SPP using a cubic interpolation routine. The respective values are presented in Table 1.

Fig. 4 shows the reduced TF cross sections for ^{8}B on ^{28}Si, ^{40}Ar and ^{58}Ni targets. TF cross section on ^{28}Si was measured at energies above the Coulomb barrier (1.6 to 2.7 times V_B). These data present a slight suppression with respect to the prediction from the barrier-penetration model. This suppression corresponds to a factor of 0.85, which is consistent with experimental data of other weakly-bound systems [5]. However, the TF data with ^{58}Ni target show a very large enhancement at near-barrier energies. This unexpected result is about a factor 2 higher than the prediction from the barrier-penetration model, and thus, inconsistent with the TF cross section for $^8\text{B} + ^{28}\text{Si}$. Our present data for the $^8\text{B} + ^{40}\text{Ar}$ system exhibit a different trend. No enhancement of the TF cross section is observed. The data are well described by the one-dimensional barrier penetration model. A similar result was obtained in a fusion experiment with the ^{17}F proton-halo nucleus [61]. This is an indication that dynamic channel coupling effects do not have a strong influence in the fusion reaction mechanism involving proton-halo systems. The results are fully consistent with the calculations here presented that predict a very small contribution of the EBU and one-proton transfer channels.

In summary, the fusion excitation function for $^8\text{B} + ^{40}\text{Ar}$ was measured with the active target technique at near-barrier energies. This novel method allows the direct identification of fusion events, which is a great advantage over previous experiments that are highly model dependent. CRC and CDCC calculations were performed to study the possible effect of direct channels not explicitly included in the CC calculations for fusion on the reaction dynamic. The TF cross section was exhausted by a single-channel calculation that only accounts for absorption due to fusion. Inelastic excitation, EBU and one-proton transfer channels have a small contribution on the TF reaction mechanism. The present data were compared with results from previous ^{8}B fusion experiments on ^{28}Si and ^{58}Ni targets and one-dimensional barrier calculations. The TF cross sections obtained for the $^8\text{B} + ^{40}\text{Ar}$ system is well described by the one-dimensional barrier penetration model, indicating no enhancement of TF cross section. These new results are consistent with the TF cross section for $^8\text{B} + ^{28}\text{Si}$ and for other weakly-bound systems.

Declaration of competing interest

The authors declare that they have no known competing financial interests or personal relationships that could have appeared to influence the work reported in this paper.

Acknowledgements

We thank the Texas A&M Cyclotron staff for their support. This work was financially supported by Fundação de Amparo à Pesquisa do Estado de São Paulo (FAPESP) under Grant Nos. 2018/04965-4, 16/17612-7 and 2019/07767-1; Conselho Nacional de Desenvolvimento Científico e Tecnológico (CNPq) Proc. No. 304961/2017-5 and INCT-FNA Proc. No. 464898/2014-5. E.N.C. thanks to PNPD/CAPES (Programa Nacional de Pós-Doutorado/CAPES) under Proc. No. 88887.475459/2020-00. S.L. thanks to the Russian Science Foundation Grant No. 17-12-01170. TexAT project was supported by the U.S. Department of Energy, Office of Science, Office of Nuclear Science, under Award No. DE-FG02-93ER40773 and by National Nuclear Security Administration, USA through the Center for Excellence in Nuclear Training and University Based Research (CENTAUR) under Grant No. DE-NA0003841.

References

[1] M. Beckerman, Sub-barrier fusion of two nuclei, Rep. Prog. Phys. 51 (8) (1988) 1047–1103, https://doi.org/10.1088/0034-4885/51/8/001.
[2] C. Iliadis, Nuclear Physics of Stars, Physics textbook, Wiley, 2008, https://books.google.com/books?id=rog9FxfGZQoC.
[3] A.G.W. Cameron, Nuclear astrophysics, Annu. Rev. Nucl. Sci. 8 (1) (1958) 299–326, https://doi.org/10.1146/annurev.ns.08.120158.001503.
[4] C. Bertulani, T. Kajino, Frontiers in nuclear astrophysics, Prog. Part. Nucl. Phys. 89 (2016) 56–100, https://doi.org/10.1016/j.ppnp.2016.04.001, http://www.sciencedirect.com/science/article/pii/S0146641016300011.
[5] L. Canto, P. Gomes, R. Donangelo, J. Lubian, M. Hussein, Phys. Rep. 596 (2015) 1–86, https://doi.org/10.1016/j.physrep.2015.08.001, http://www.sciencedirect.com/science/article/pii/S0370157315003385.
[6] L. Canto, P. Gomes, R. Donangelo, M. Hussein, Fusion and breakup of weakly bound nuclei, Phys. Rep. 424 (1) (2006) 1–111, https://doi.org/10.1016/j.physrep.2005.10.006, http://www.sciencedirect.com/science/article/pii/S037015730500459X.
[7] N. Keeley, R. Raabe, N. Alamanos, J. Sida, Fusion and direct reactions of halo nuclei at energies around the Coulomb barrier, Prog. Part. Nucl. Phys. 59 (2) (2007) 579–630, https://doi.org/10.1016/j.ppnp.2007.02.002, http://www.sciencedirect.com/science/article/pii/S0146641007000397.
[8] M. Dasgupta, et al., Fusion versus breakup: observation of large fusion suppression for $^9Be+^{208}$Pb, Phys. Rev. Lett. 82 (1999) 1395–1398, https://doi.org/10.1103/PhysRevLett.82.1395, https://link.aps.org/doi/10.1103/PhysRevLett.82.1395.
[9] M. Dasgupta, et al., Effect of breakup on the fusion of ^{6}Li, ^{7}Li, and ^{9}Be with heavy nuclei, Phys. Rev. C 70 (2004) 024606, https://doi.org/10.1103/PhysRevC.70.024606, https://link.aps.org/doi/10.1103/PhysRevC.70.024606.
[10] D. Chattopadhyay, et al., Role of cluster structure in the breakup of ^{7}Li, Phys. Rev. C 97 (2018) 051601, https://doi.org/10.1103/PhysRevC.97.051601, https://link.aps.org/doi/10.1103/PhysRevC.97.051601.

[11] A. Mukherjee, et al., Influence of projectile a-breakup threshold on complete fusion, Phys. Lett. B 636 (2) (2006) 91–95, https://doi.org/10.1016/j.physletb.2006.03.051, http://www.sciencedirect.com/science/article/pii/S0370269306003844.

[12] P.R.S. Gomes, et al., Comprehensive study of reaction mechanisms for the ^{9}Be $+^{144}$ Sm system at near- and sub-barrier energies, Phys. Rev. C 73 (2006) 064606, https://doi.org/10.1103/PhysRevC.73.064606, https://link.aps.org/doi/10.1103/PhysRevC.73.064606.

[13] K.J. Cook, et al., Origins of incomplete fusion products and the suppression of complete fusion in reactions of ^{7}Li, Phys. Rev. Lett. 122 (2019) 102501, https://doi.org/10.1103/PhysRevLett.122.102501, https://link.aps.org/doi/10.1103/PhysRevLett.122.102501.

[14] M. Fisichella, et al., Breakup and n-transfer effects on the fusion reactions ^{6,7}Li $+^{120,119}$ Sn around the Coulomb barrier, Phys. Rev. C 95 (2017) 034617, https://doi.org/10.1103/PhysRevC.95.034617, https://link.aps.org/doi/10.1103/PhysRevC.95.034617.

[15] K.J. Cook, et al., Importance of lifetime effects in breakup and suppression of complete fusion in reactions of weakly bound nuclei, Phys. Rev. C 93 (2016) 064604, https://doi.org/10.1103/PhysRevC.93.064604, https://link.aps.org/doi/10.1103/PhysRevC.93.064604.

[16] R. Kumar, J.A. Lay, A. Vitturi, Enhanced subbarrier fusion for proton halo nuclei, Phys. Rev. C 89 (2014) 027601, https://doi.org/10.1103/PhysRevC.89.027601, https://link.aps.org/doi/10.1103/PhysRevC.89.027601.

[17] J. Lubian, T. Correa, P.R.S. Gomes, L.F. Canto, Effect of breakup on fusion cross sections of the ^{8}B + ^{58}Ni system by means of quasi-elastic angular distributions, Phys. Rev. C 78 (2008) 064615, https://doi.org/10.1103/PhysRevC.78.064615, https://link.aps.org/doi/10.1103/PhysRevC.78.064615.

[18] L.F. Canto, P.R.S. Gomes, J. Lubian, L.C. Chamon, E. Crema, Disentangling static and dynamic effects of low breakup threshold in fusion reactions, J. Phys. G, Nucl. Part. Phys. 36 (1) (2008) 015109, https://doi.org/10.1088/0954-3899/36/1/015109.

[19] L. Canto, P. Gomes, J. Lubian, L. Chamon, E. Crema, Dynamic effects of breakup on fusion reactions of weakly bound nuclei, Nucl. Phys. A 821 (1) (2009) 51–71, https://doi.org/10.1016/j.nuclphysa.2009.02.001, http://www.sciencedirect.com/science/article/pii/S0375947409001092.

[20] V. Scuderi, et al., Fusion and direct reactions for the system ^{6}He + ^{64}Zn at and below the Coulomb barrier, Phys. Rev. C 84 (2011) 064604, https://doi.org/10.1103/PhysRevC.84.064604, https://link.aps.org/doi/10.1103/PhysRevC.84.064604.

[21] Y.E. Penionzhkevich, et al., Excitation functions of fusion reactions and neutron transfer in the interaction of 6He with 197Au and 206Pb, Eur. Phys. J. A 31 (2007) 185, https://doi.org/10.1140/epja/i2006-10166-9.

[22] A.M. Vinodkumar, et al., Interaction of ^{11}Li with ^{208}Pb, Phys. Rev. C 87 (2013) 044603, https://doi.org/10.1103/PhysRevC.87.044603, https://link.aps.org/doi/10.1103/PhysRevC.87.044603.

[23] D.J. Hinde, M. Dasgupta, Systematic analysis of above-barrier fusion of ^{9,10,11}Be $+^{209}$ Bi, Phys. Rev. C 81 (2010) 064611, https://doi.org/10.1103/PhysRevC.81.064611, https://link.aps.org/doi/10.1103/PhysRevC.81.064611.

[24] A. Lemasson, et al., Modern Rutherford experiment: tunneling of the most neutron-rich nucleus, Phys. Rev. Lett. 103 (2009) 232701, https://doi.org/10.1103/PhysRevLett.103.232701, https://link.aps.org/doi/10.1103/PhysRevLett.103.232701.

[25] V. Guimarães, et al., Nuclear and Coulomb interaction in ^{8}B breakup at sub-Coulomb energies, Phys. Rev. Lett. 84 (2000) 1862–1865, https://doi.org/10.1103/PhysRevLett.84.1862, https://link.aps.org/doi/10.1103/PhysRevLett.84.1862.

[26] F.M. Nunes, I.J. Thompson, Multistep effects in sub-Coulomb breakup, Phys. Rev. C 59 (1999) 2652–2659, https://doi.org/10.1103/PhysRevC.59.2652, https://link.aps.org/doi/10.1103/PhysRevC.59.2652.

[27] A. Pakou, et al., Fusion cross sections of ^{8}b + ^{28}Si at near-barrier energies, Phys. Rev. C 87 (2013) 014619, https://doi.org/10.1103/PhysRevC.87.014619, https://link.aps.org/doi/10.1103/PhysRevC.87.014619.

[28] E.F. Aguilera, et al., Near-barrier fusion of the ^{8}**B** $+^{58}$ Ni proton-halo system, Phys. Rev. Lett. 107 (2011) 092701, https://doi.org/10.1103/PhysRevLett.107.092701, https://link.aps.org/doi/10.1103/PhysRevLett.107.092701.

[29] R. Tribble, R. Burch, C. Gagliardi, Mars: a momentum achromat recoil spectrometer, Nucl. Instrum. Methods Phys. Res., Sect. A 285 (3) (1989) 441–446, https://doi.org/10.1016/0168-9002(89)90215-5, http://www.sciencedirect.com/science/article/pii/0168900289902155.

[30] E. Koshchiy, et al., Texas Active Target (TexAT) detector for experiments with rare isotope beams, Nucl. Instrum. Methods Phys. Res., Sect. A 957 (2020) 163398, https://doi.org/10.1016/j.nima.2020.163398, http://www.sciencedirect.com/science/article/pii/S0168900220300073.

[31] Y. Giomataris, P. Rebourgeard, J. Robert, G. Charpak, Micromegas: a high-granularity position-sensitive gaseous detector for high particle-flux environments, Nucl. Instrum. Methods Phys. Res., Sect. A 376 (1) (1996) 29–35, https://doi.org/10.1016/0168-9002(96)00175-1, http://www.sciencedirect.com/science/article/pii/0168900296001751.

[32] S. Biagi, A multiterm Boltzmann analysis of drift velocity, diffusion, gain and magnetic-field effects in argon-methane-water-vapour mixtures, Nucl. Instrum. Methods Phys. Res., Sect. A 283 (3) (1989) 716–722, https://doi.org/10.1016/0168-9002(89)91446-0, http://www.sciencedirect.com/science/article/pii/0168900289914460.

[33] M.A. Fischler, R.C. Bolles, Random sample consensus: a paradigm for model fitting with applications to image analysis and automated cartography, Commun. ACM 24 (1981) 381–395.

[34] J. Zamora, G. Fortino, Tracking algorithms for TPCs using consensus-based robust estimators, Nucl. Instrum. Methods Phys. Res., Sect. A 988 (2021) 164899, https://doi.org/10.1016/j.nima.2020.164899, https://www.sciencedirect.com/science/article/pii/S0168900220312961.

[35] Y. Ayyad, W. Mittig, D. Bazin, S. Beceiro-Novo, M. Cortesi, Novel particle tracking algorithm based on the Random Sample Consensus Model for the Active Target Time Projection Chamber (AT-TPC), Nucl. Instrum. Methods Phys. Res., Sect. A 880 (2018) 166–173, https://doi.org/10.1016/j.nima.2017.10.090, http://www.sciencedirect.com/science/article/pii/S0168900217311798.

[36] A. Matta, et al., NPTOOL, framework, http://nptool.org/.

[37] J. Bishop, et al., State of the art measurements with TexAT, J. Phys. Conf. Ser. 1308 (2019) 012006, https://doi.org/10.1088/1742-6596/1308/1/012006.

[38] J. Kolata, et al., Fusion studies with low-intensity radioactive ion beams using an active-target time projection chamber, Nucl. Instrum. Methods Phys. Res., Sect. A 830 (2016) 82–87, https://doi.org/10.1016/j.nima.2016.05.036, http://www.sciencedirect.com/science/article/pii/S0168900216304181.

[39] J.J. Kolata, E.F. Aguilera, V. Guimarães, Near and sub-barrier reactions of 8B, EPJ Web Conf. 163 (2017) 00031, https://doi.org/10.1051/epjconf/201716300031.

[40] E. Pollacco, et al., Get: a generic electronics system for TPCs and nuclear physics instrumentation, Nucl. Instrum. Methods Phys. Res., Sect. A 887 (2018) 81–93, https://doi.org/10.1016/j.nima.2018.01.020, http://www.sciencedirect.com/science/article/pii/S0168900218300342.

[41] SRIM code, http://www.srim.org/.

[42] NIST Chemistry WebBook, https://webbook.nist.gov/chemistry/.

[43] I.J. Thompson, Coupled reaction channels calculations in nuclear physics, Comput. Phys. Rep. 7 (4) (1988) 167–212, https://doi.org/10.1016/0167-7977(88)90005-6, http://www.sciencedirect.com/science/article/pii/0167797788900056.

[44] L.C. Chamon, et al., Toward a global description of the nucleus-nucleus interaction, Phys. Rev. C 66 (2002) 014610, https://doi.org/10.1103/PhysRevC.66.014610, https://link.aps.org/doi/10.1103/PhysRevC.66.014610.

[45] L.F. Canto, R. Donangelo, M.S. Hussein, P. Lotti, J. Lubian, J. Rangel, Theoretical considerations about heavy-ion fusion in potential scattering, Phys. Rev. C 98 (2018) 044617, https://doi.org/10.1103/PhysRevC.98.044617, https://link.aps.org/doi/10.1103/PhysRevC.98.044617.

[46] S. Raman, C. Nestor, P. Tikkanen, Transition probability from the ground to the first-excited 2+ state of even–even nuclides, At. Data Nucl. Data Tables 78 (1) (2001) 1–128, https://doi.org/10.1006/adnd.2001.0858, http://www.sciencedirect.com/science/article/pii/S009260X01908587.

[47] J. Lubian, F.M. Nunes, Searching for a polarization potential in the breakup of 8B, J. Phys. G, Nucl. Part. Phys. 34 (3) (2007) 513–521, https://doi.org/10.1088/0954-3899/34/3/009.

[48] A. Barioni, et al., Elastic scattering and total reaction cross sections for the ^{8}B, ^{7}Be, and ^{6}Li $+^{12}$C systems, Phys. Rev. C 84 (2011) 014603, https://doi.org/10.1103/PhysRevC.84.014603, https://link.aps.org/doi/10.1103/PhysRevC.84.014603.

[49] J. Rangel, J. Lubian, L.F. Canto, P.R.S. Gomes, Effect of Coulomb breakup on the elastic cross section of the ^{8}B proton-halo projectile on a heavy, ^{208}Pb target, Phys. Rev. C 93 (2016) 054610, https://doi.org/10.1103/PhysRevC.93.054610, https://link.aps.org/doi/10.1103/PhysRevC.93.054610.

[50] W.D.M. Rae, NuShellX, http://www.garsington.eclipse.co.uk.

[51] C.H. Dasso, M. Lozano, A. Vitturi, Tunneling phenomena in the presence of kinematically forbidden channels, Phys. Rev. A 44 (1991) 4743–4746, https://doi.org/10.1103/PhysRevA.44.4743, https://link.aps.org/doi/10.1103/PhysRevA.44.4743.

[52] A.M. Moro, et al., Coupling to breakup channels using a transformed harmonic oscillator basis, Phys. Rev. C 65 (2001) 011602, https://doi.org/10.1103/PhysRevC.65.011602, https://link.aps.org/doi/10.1103/PhysRevC.65.011602.

[53] K. Ogata, K. Yoshida, Applicability of the continuum-discretized coupled-channels method to the deuteron breakup at low energies, Phys. Rev. C 94 (2016) 051603, https://doi.org/10.1103/PhysRevC.94.051603, https://link.aps.org/doi/10.1103/PhysRevC.94.051603.

[54] Y. Chazono, K. Yoshida, K. Ogata, Examination of the adiabatic approximation for (d, p) reactions, Phys. Rev. C 95 (2017) 064608, https://doi.org/10.1103/PhysRevC.95.064608, https://link.aps.org/doi/10.1103/PhysRevC.95.064608.

[55] V.V. Sargsyan, G.G. Adamian, N.V. Antonenko, W. Scheid, H.Q. Zhang, Influence of neutron transfer in reactions with weakly and strongly bound nuclei on the sub-barrier capture process, Phys. Rev. C 86 (2012) 014602, https://doi.org/10.1103/PhysRevC.86.014602, https://link.aps.org/doi/10.1103/PhysRevC.86.014602.

[56] V.V. Sargsyan, G.G. Adamian, N.V. Antonenko, W. Scheid, H.Q. Zhang, Sub-barrier capture reactions with ^{16,18}O and ^{40,48}Ca beams, Eur. Phys. J. A 49 (2013) 54, https://doi.org/10.1140/epja/i2013-13054-3.

[57] V.A. Rachkov, A.V. Karpov, A.S. Denikin, V.I. Zagrebaev, Examining the enhancement of sub-barrier fusion cross sections by neutron transfer with positive q values, Phys. Rev. C 90 (2014) 014614, https://doi.org/10.1103/PhysRevC.90.014614, https://link.aps.org/doi/10.1103/PhysRevC.90.014614.

[58] V.V. Sargsyan, G.G. Adamian, N.V. Antonenko, W. Scheid, H.Q. Zhang, Examination of the different roles of neutron transfer in the sub-barrier fusion reactions $^{32}S + ^{94,96}Zr$ and $^{40}Ca + ^{94,96}Zr$, Phys. Rev. C 91 (2015) 014613, https://doi.org/10.1103/PhysRevC.91.014613, https://link.aps.org/doi/10.1103/PhysRevC.91.014613.

[59] C.Y. Wong, Interaction barrier in charged-particle nuclear reactions, Phys. Rev. Lett. 31 (1973) 766–769, https://doi.org/10.1103/PhysRevLett.31.766, https://link.aps.org/doi/10.1103/PhysRevLett.31.766.

[60] E.F. Aguilera, et al., Above-barrier fusion enhancement of proton-halo systems, Phys. Rev. C 93 (2016) 034613, https://doi.org/10.1103/PhysRevC.93.034613, https://link.aps.org/doi/10.1103/PhysRevC.93.034613.

[61] K.E. Rehm, et al., Fusion cross sections for the proton drip line nucleus ^{17}f at energies below the Coulomb barrier, Phys. Rev. Lett. 81 (1998) 3341–3344, https://doi.org/10.1103/PhysRevLett.81.3341, https://link.aps.org/doi/10.1103/PhysRevLett.81.3341.